Journal of the Brazilian Society of Mechanical Sciences and Engineering (2026) 48:293
https://doi.org/10.1007/s40430-026-06346-1

TECHNICAL PAPER

Forced nonlinear oscillations of a cylindrical panel resting on a discontinuous unilateral elastic base

Jordana L. Morais[1] · **Frederico M. A. Silva**[1]

Received: 4 January 2025 / Accepted: 14 January 2026 / Published online: 21 March 2026

Abstract

The aim of this work is to analytically investigate the influence of a discontinuous unilateral elastic base on the nonlinear resonance curves of imperfect cylindrical panels. To achieve this, the set of partial differential nonlinear equilibrium equations representing the imperfect cylindrical panel is complemented with a transversal equilibrium equation derived from Donnell's nonlinear shallow shell theory and Airy's stress function. To discretize this set of equations, a standard Galerkin method is applied, using a particular modal solution for the transversal displacement field that includes simply supported boundary conditions, which can represent the nonlinear modal coupling commonly present in the dynamic behavior of cylindrical panels. The effects of the discontinuous unilateral elastic base are directly inserted into the equilibrium equation by using the Heaviside and signum functions to represent the reaction of the elastic base. From the set of discretized equilibrium equations, the nonlinear resonance curves, phase portraits and Poincaré section mapping are obtained via several numerical strategies. The results presented here demonstrate that the unilateral contact of the elastic base significantly changes the dynamic behavior of the imperfect cylindrical panel by creating several bifurcation points that give rise to quasiperiodic responses. These also modify the stability along the resonance curves compared with the case where the elastic base is considered to be bilateral. This work contributes to the nonlinear dynamic analysis of imperfect cylindrical panels with discontinuous unilateral elastic foundations, and introduces a novel evaluation of bifurcation sequences and stability of resonance curves using a non-smooth contact model.

Keywords Unilateral contact · Resonance curves · Cylindrical panel · Initial geometric imperfections

1 Introduction

Slender structures in contact with an elastic base or internal elastic support can be used in several applications in different engineering fields to describe soil–structure interactions [1–5]. Circular cylindrical shells and open circular cylindrical shells (cylindrical panels) are slender structures that can interact with an elastic base, and scholars have investigated their static and dynamic behavior over the years. An overview of published work on the static and dynamic behavior of plates and shells subjected to different applications, loads and interactions with different media can be found in the reviews in [6–10].

In some structural applications, cylindrical shells may interact with an elastic base that exerts an additional reaction force upon their assumption of equilibrium. This reaction force deserves attention in view of its ability to resist displacements of the shells, which may be via bilateral or unilateral contact. The influence of constitutive models of the bilateral elastic response on the free vibration [11–14] and forced nonlinear [15–19] response of cylindrical shells has previously been investigated, and the influence of the stiffness parameters and the contact region of the bilateral elastic response on the static and dynamic nonlinear behavior of the shells has been demonstrated.

The works cited above highlight the influence of the stiffness and contact region in bilateral elastic foundations on the vibration behavior of different structures. By extending

Technical Editor: Pedro Manuel Calas Lopes Pacheco.

✉ Frederico M. A. Silva
silvafma@ufg.br

Jordana L. Morais
jordanalopes@discente.ufg.br

[1] School of Civil and Environmental Engineering, Federal University of Goiás, UFG, Av. Universitária, No. 1488, Setor Universitário, Goiás, GO 74605-220, Brazil

these findings, the present work advances current knowledge by considering unilateral and discontinuous contact. This model allows for a more realistic prediction of nonlinear dynamic responses, including resonance shifts and complex bifurcations, in systems where contact conditions are not continuously maintained. The global stiffness of the structural system is dependent on the displacement of the elastic base, which in turn can change the static and dynamic structural response. From this dependence on displacement, the equilibrium equations of the structural problem can be expressed as a classical piecewise problem [20, 21], a formulation that has received attention in the literature. Lancioni and Lenci [22] reported that unilateral springs significantly affect the motion of a semi-infinite beam at higher frequencies, and demonstrated that the superharmonic wave dominates the primary harmonic wave. Lenci and Clementi [23] found that compared with bilateral foundations, unilateral contact alters the wave velocity in an infinite beam. Coskun and Engin [24] analyzed the nonlinear vibrations of a beam on a tensionless Winkler foundation, and used perturbation techniques to analyze the resulting contact and noncontact regions. Bhattiprolu et al. [25] conducted a dynamic analysis of a beam with unilateral contact on viscoelastic foundations, and applied the harmonic balance method to build a predictive model that incorporated nonlinear interactions. Panahandeh-Shahraki and Mirdamadi [26] explored the thermal buckling of composite curved panels under unilateral constraints, and reported that the foundation plays a crucial role in determining stability under thermal loads. Silveira et al. [27] presented a semi-analytical Ritz-type methodology for nonlinear static analysis of unilateral contact problems in beams, columns, and arches resting on a tensionless Winkler-type elastic foundation. Vestroni and coworkers carried out a numerical investigation of beams with cracks or systems hitting elastic obstacles via nonlinear normal modes, and an experimental investigation of a vibrating system with piecewise linear characteristics [28–30]. It was observed in [22–30] that the presence of a unilateral contact between the elastic base and foundation significantly influences both the structural stiffness and oscillatory behavior. This effect, which depends on the structural displacement, leads to notable changes in the structural response and stability. These studies reinforce the importance of modeling unilateral contact in structural systems with elastic foundations, since non-smooth interactions such as these directly affect the stiffness, oscillatory behavior, and stability, thus providing theoretical and numerical evidence that the dynamic response is highly sensitive to the displacement-dependent activation of the elastic base.

Based on these previous studies, the present work extends this analysis to imperfect cylindrical panels, and highlights how discontinuous contact influences the resonance curves, bifurcation phenomena, and stability boundaries. This contributes to a better understanding of nonlinear vibrations in structures with localized asymmetric and antisymmetric elastic non-smooth media. Recently, Morais and Silva [31] investigated the nonlinear free vibrations of imperfect cylindrical panels in contact with a unilateral Winkler elastic base. These authors explored the influence of the region of application of the elastic base, the magnitude of the initial geometric imperfections, and the unilateral contact on the natural frequencies and backbone curves (frequency–amplitude relation) of the cylindrical panels. In the present work, we carry out a nonlinear dynamic analysis of an imperfect cylindrical panel harmonically excited by a transverse load, and extend previous work to evaluate the sequence of bifurcation and the stability of the nonlinear resonance curves. To do this, the nonlinear equilibrium equation for the imperfect cylindrical panel is described by Donnell's nonlinear shallow shell theory, and is discretized by the Galerkin method, in which a consistent modal expansion is used for the transversal field displacement [31, 32]. The discontinuous unilateral elastic base is governed by the Winkler constitutive law, associated with the Heaviside and signum functions, which represent the discontinuous region and the unilateral contact of the elastic base, respectively. Discretized nonlinear second-order differential equilibrium equations are employed, using various numerical strategies, to compute the nonlinear resonance curves along with their associated stability and bifurcation points, phase portraits, and Poincaré section mappings. This approach enables a comprehensive analysis of the influence of discontinuous unilateral elastic foundations on the dynamic behavior of the cylindrical panel, thus contributing to a nonlinear dynamic analysis of imperfect cylindrical panels with discontinuous unilateral elastic foundations. A novel evaluation method for bifurcation sequences and the stability of resonance curves is introduced based on a non-smooth contact model.

2 Problem formulation

2.1 Cylindrical panel equations

Figure 1 shows a thin circular cylindrical panel with radius R, thickness h, axial length a_x, circumferential length a_θ, and open angle $\Theta[=a_\theta/R]$. It is assumed to be made of a linear elastic, isotropic, and homogenous material, with Young's modulus E, Poisson's coefficient ν, and density ρ. It is also considered to have an elastic base that can be internally positioned within the domain of the panel and in different regions. In Fig. 1, the parameters $\varepsilon_{i,j}$ ($i=1, \ldots, N$ and $j=1, \ldots, 4$) represent the corners of the rectangular domain of the elastic base, which are used to formulate the contact with

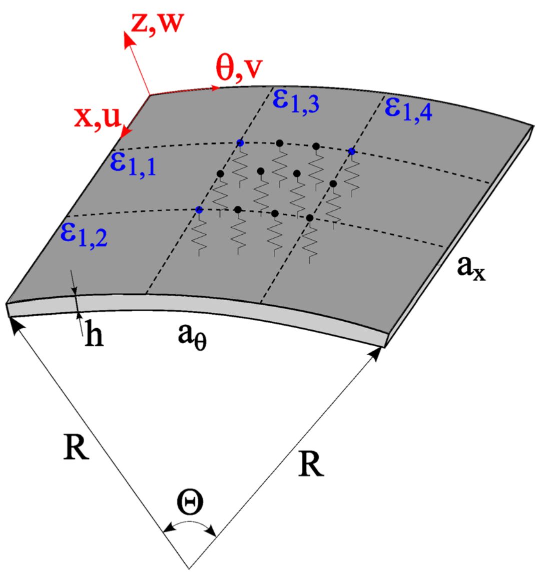

Fig. 1 Geometry and displacement fields for a cylindrical panel with an elastic base positioned in the longitudinal direction $0 \le \varepsilon_{1,1} < \varepsilon_{1,2} \le a_x$ and in the circumferential direction $0 \le \varepsilon_{1,3} < \varepsilon_{1,4} \le \Theta$

the *i*-th region of the elastic base. The displacement fields in the axial (u), circumferential (v), and transverse (w) directions, with their respective cylindrical coordinates x, θ, and z, are also shown in Fig. 1. An initial geometrical imperfection w_0 in the transverse direction of the panel is also considered in this work.

To obtain the nonlinear equilibrium and compatibility and continuity equations, the deformation fields and the changes in the curvature of the middle surface of an imperfect cylindrical panel are assumed to obey Donnell's nonlinear shallow shell theory [33, 34]. In this theory [33], six assumptions are made: (i) the structure is thin, i.e., $h \ll R$ and $h \ll a_x$; (ii) the transverse displacement field is small compared with R and a_x; (iii) the mid-surface rotation is small, with $|w_{,x}| \ll 1$ and $|w_{,\theta}/R| \ll 1$; (iv) the deformation components are small, allowing for linear elasticity; (v) the stresses normal to the mid-surface panel are negligible, with deformation varying linearly along the thickness, thus maintaining the undeformed mid-surface as straight and normal; and (vi) the tangential displacements u and v are infinitesimal, and the deformation fields retain only nonlinear terms that depend on w. As a result, transverse shear and rotary inertia are neglected, and the cylindrical panel can be modeled using the displacement fields u, v and w [35]. Since the in-plane inertia is neglected, the nonlinear equilibrium equations depend solely on the transverse displacement and Airy's stress function f [33], thus simplifying the degrees of freedom of the system, i.e.,

$$\begin{aligned} &\rho h\ddot{w} + 2\eta_1\rho h\omega_0\dot{w} + D\nabla^4 w - f_{,\theta\theta}(w_{,x} + w_{0,x})_{,x} + Rf_{,xx} \\ &- f_{,xx}(w_{,\theta} + w_{0,\theta})_{,\theta} - 2f_{x\theta}\left(w_{,\theta x} + w_{0,\theta x}\right) + p_k + p(t) = 0 \end{aligned} \quad (1)$$

$$\nabla^4 f = \frac{Eh}{R^4}\left(w_{,x\theta}^2 - w_{,xx}w_{,\theta\theta} + Rw_{,xx} + 2w_{,x\theta}w_{0,x\theta} - \left(w_{,xx}w_{0,\theta\theta} - w_{,\theta\theta}w_{0,xx}\right)\right) \quad (2)$$

where $D[=Eh^3/12(1-\nu^2)]$ is the flexural stiffness, $_1$ is the viscous damping factor, p_k is the reaction of the elastic base, $p(t)$ is a transversal time-dependent load, and

$$\nabla^4\left(\right) = \left(\right)_{,xxxx} + \frac{2}{R^2}\left(\right)_{,\theta\theta xx} + \frac{1}{R^4}\left(\right)_{,\theta\theta\theta\theta} \quad (3)$$

where ∇^4 is the biharmonic differential operator.

The cylindrical panel is considered to be simply supported at each of the edges. Thus, the in-plane boundary conditions are satisfied by Airy's stress function [33], and the transversal geometric boundary conditions are as follows:

$$\begin{aligned} &w\left(0,\theta\right) = w\left(a_x,\theta\right) = w\left(x,0\right) = w\left(x,\Theta\right) = 0 \\ &M_x\left(0,\theta\right) = M_x\left(a_x,\theta\right) = M_\theta\left(x,0\right) = M_\theta\left(x,\Theta\right) = 0 \end{aligned} \quad (4)$$

The time-dependent transverse load $p(t)$ directly excites the fundamental vibration mode (m, n) of the simply supported cylindrical panel. To represent this, $p(t)$ is assumed to be as follows:

$$p\left(t\right) = P\sin\left(\frac{n\pi\theta}{\Theta}\right)\sin\left(\frac{m\pi x}{a_x}\right)cos\left(\omega t\right) \quad (5)$$

where P and ω are the amplitude and the excitation frequency of the lateral load, respectively, and m and n are the half-wavenumbers of the fundamental mode of vibration of the cylindrical panel in the longitudinal and circumferential directions, respectively.

2.2 Reaction of the elastic base and its contact hypotheses with an imperfect cylindrical panel

In this study, we analyze a cylindrical panel in contact with either an elastic medium or an internal elastic boundary condition, which may be partially embedded within the panel structure and is subject to a unilateral constraint. The associated elastic reaction force, P_k, is defined as follows:

$$p_k = K_w H_x H_\theta \frac{\left(1 - sgnw_r\right)}{2} w \quad (6)$$

where w_r represents the transverse displacement of the imperfect panel, capturing two possible contact configurations with the elastic foundation; K_w denotes the Winkler stiffness parameter; H_x and H are Heaviside functions, which define the domain of the foundation; and the signum function, *sgn*, controls the unilateral contact response.

In Eq. (6), the product of the Heaviside functions ($H_x H_\theta$) is used to delimit the elastic base region. The parameters

$0 \le \varepsilon_{i,1} < \varepsilon_{i,2} \le a_x$ define the region in which the i-th elastic base acts in the longitudinal direction, whereas the parameters $0 \le \varepsilon_{i,3} < \varepsilon_{i,4} \le \Theta$ circumferentially determine the i-th elastic base region. The product of these Heaviside functions is expressed as follows:

$$H_x H_\theta = \sum_{i=1}^{N} \left[H\left(x-\varepsilon_{i,1}\right)-H\left(x-\varepsilon_{i,2}\right)\right]\left[H\left(\theta-\varepsilon_{i,3}\right)-H\left(\theta-\varepsilon_{i,4}\right)\right] \quad (7)$$

where N represents the number of regions with elastic bases.

In this work, the reaction of the elastic base exists only when it is compressed, i.e., the elastic base exerts a unilateral contact on the cylindrical panel. To represent this, we consider the signum function, sgn, in Eq. (6), which returns + 1 or − 1 depending on the signal of the argument w_r. Thus, when w_r assumes positive values, the term $(1 - sgn\ w_r)/2$ in Eq. (6) results in zero, taking p_k to zero. Otherwise, when w_r assumes negative values, the term $(1 - sgn\ w_r)/2$ in Eq. (6) results in unity, and the elastic base reaction p_k is fully considered in the equilibrium equation. This approach avoids the need for an evaluation of the contact between the elastic base and the cylindrical panel with external numerical routines or additional equilibrium equations. For comparison purposes, we define an elastic base with bilateral contact (i.e., the elastic base's reaction occurs in both directions of w_r) by replacing the term $(1 - sgn\ w_r)/2$ in Eq. (6) with unity.

We now examine the argument w_r appearing in Eq. (6), which allows for the consideration of two hypotheses regarding the simultaneous influence of initial geometric imperfections and the presence of a unilateral elastic foundation, as illustrated in Fig. 2.

In Hypothesis 1 (Fig. 2a), a circumferential section of an imperfect cylindrical panel is considered, characterized by a positive amplitude of the imperfection (continuous blue line), while the elastic foundation is initially configured to match the shape of a perfect panel (dashed black line). In this configuration, a gap exists between the imperfect panel and the elastic foundation. Hence, Eq. (6) is evaluated using $w_r = w + w_0$, indicating that the perfect panel configuration serves as the reference for computing the work done by the elastic base. This hypothesis is particularly relevant in the context of nonlinear vibrations of cylindrical panels: during transverse oscillations (represented by the continuous magenta line in Fig. 2a), the displacement w may remain smaller than the initial gap, and contact with the elastic foundation does not occur. Contact only takes place if the negative oscillation amplitude of w exceeds the magnitude of the imperfection.

In Hypothesis 2 (Fig. 2b), it is assumed that the elastic foundation is perfectly coupled to the imperfect cylindrical panel with a positive imperfection amplitude (continuous blue line). In this case, the term $w_r = w$ is used in Eq. (6), thereby eliminating the initial gap and ensuring continuous contact. In this case, the imperfect panel configuration becomes the reference for evaluating the work done by the elastic base. Consequently, contact occurs for all negative values of the transverse displacement field w.

For negative imperfection amplitudes, the imperfect panel (continuous blue line) remains in contact with the elastic foundation at the reference configuration in both hypotheses, as shown in Fig. 2c. Loss of contact only occurs during oscillations in the positive direction of the transverse displacement w.

The contact between the elastic base and the imperfect cylindrical panel introduces a discontinuity in the structural stiffness due to the nonlinear, piecewise nature of the unilateral contact behavior. This discontinuity influences both the frequency of the forced response and the amplitude of oscillation, and may affect the panel's dynamic stability.

2.3 Discretization of the nonlinear equilibrium equation for the cylindrical panel

To obtain a discrete model for an imperfect cylindrical panel with a discontinuous unilateral elastic base, a transverse displacement field w is chosen to discretize the nonlinear partial differential transversal equilibrium equation into a set of nonlinear ordinary differential equilibrium equations.

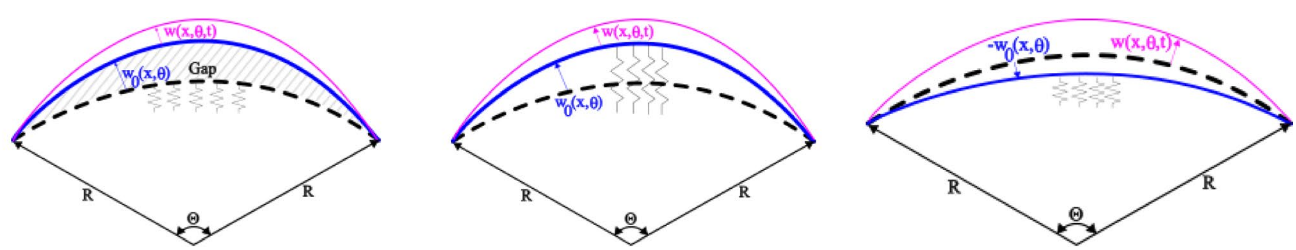

(a) Hypothesis 1 (positive magnitude of the imperfection) (b) Hypothesis 2 (positive magnitude of the imperfection) (c) Negative magnitude of the imperfection

Fig. 2 Circumferential section of the cylindrical panel, illustrating the contact scenarios between the unilateral elastic foundation and the imperfect cylindrical panel: **a**, **b** positive and **c** negative imperfection magnitudes (- -perfect panel, blue straight line imperfect panel, pink straight line panel during oscillation). $w_0(x, \theta)$ represents the initial geometric imperfection, while $w(x, \theta, t)$ denotes the dynamic displacement

This choice must be carefully made to correctly represent the nonlinear modal coupling and the nonlinear mechanical behavior of the cylindrical shells and panels [36–40]. In this study, the transverse displacement field used was derived from the perturbation method [41], which has been applied to several dynamic problems involving cylindrical shells and panels [18, 32, 42–46]. The perturbation method starts by considering the fundamental vibration mode of the cylindrical panel as the initial solution, and then takes into account the boundary geometric condition of the cylindrical panel to derive a general transversal displacement field. For more details about the application of the perturbation method to shells, see [41]. Using this approach, the following general solution for the transversal displacement field of the simply supported cylindrical panel is obtained, which considers the nonlinear modal coupling and modal interaction between the modes [35, 39, 47, 48] presented in the nonlinear equilibrium equation:

$$\begin{aligned} w = & \sum_{m=1,2,\ldots} \sum_{n=1,2,\ldots} \sum_{i=1,2,3\ldots} \sum_{j=1,2,3\ldots} A_{im,jn}(t) \sin\left(\frac{im\pi x}{a_x}\right) \sin\left(\frac{jn\pi\theta}{\Theta}\right) \\ & + \sum_{m=1,2,\ldots} \sum_{n=1,2,\ldots} \sum_{\alpha=0,1,2,3\ldots} \sum_{\beta=0,1,2,3\ldots} B_{(2+6\alpha)m,(2+6\beta)n}(t) \left\{ \left[\frac{3+6\alpha}{4+12\alpha} \cos\left(\frac{6\alpha m\pi x}{a_x}\right) \right.\right. \\ & \left. - \cos\left(\frac{(2+6\alpha)m\pi x}{a_x}\right) + \frac{1+6\beta}{4+12\beta} \cos\left(\frac{(4+6\alpha)m\pi x}{a_x}\right) \right] \\ & \left.\left[\frac{3+6\beta}{4+12\beta} \cos\left(\frac{6\beta n\pi\theta}{\Theta}\right) - \cos\left(\frac{(2+6\beta)n\pi\theta}{\Theta}\right) + \frac{1+6\beta}{4+12\beta} \cos\left(\frac{(4+6\beta)n\pi\theta}{\Theta}\right) \right] \right\} \end{aligned} \tag{8}$$

where $A_{im,jn}(t)$ and $B_{(2+6\alpha)m,(2+6\beta)n}(t)$ are the modal amplitudes of the transverse displacement field.

The initial geometric imperfection, w_0, in the shape of the first vibration mode of the cylindrical panel is defined as follows:

$$w_0 = w_0^{imp} h \sin\left(\frac{m\pi x}{a_x}\right) \sin\left(\frac{n\pi\theta}{\Theta}\right) \tag{9}$$

where w_0^{imp} is the amplitude of the initial geometric imperfection in relation to the thickness of the cylindrical panel.

3 Numerical results

In this section, we present a nonlinear forced and damped vibration analysis of a simply supported imperfect cylindrical panel in contact with a unilateral elastic base. The cylindrical panel has a radius of curvature R = 8.333 m, thickness h = 0.01 m, axial length a_x = 1.0 m and circumferential length a_θ = 1.0 m. The material is linearly elastic, isotropic and homogeneous, with a modulus of elasticity E = 210 GPa, Poisson's ratio v = 0.3 and density r = 7800 kg/m^3. It is noteworthy that the geometric and physical parameters considered in this work do not correspond to a specific engineering application but were selected based on previous studies by the authors [31, 32]. This provides a simplified yet representative framework for investigating fundamental aspects of nonlinear dynamic behavior, thereby allowing for a deeper understanding of the underlying mechanisms before more complex real-world cases are addressed.

In this study, we investigate cylindrical panels with discontinuous elastic bases applied in different areas of the panel. Figure 3 shows the two different locations for the elastic base. Elastic Base 1 (Fig. 3a) shows an elastic base centered in one quadrant of the cylindrical panel (Q2), while Elastic Base 2 (Fig. 3b) represents an elastic base centered in two opposite quadrants (Q2 - Q4). For each case, we consider three values of the variation in the contact area of the elastic base in relation to the area of the cylindrical panel, which are 7.5%, 10.0% and 12.5%. Table 1 gives the limits used in the Heaviside functions in Eq. (7) to define each case for the elastic base shown in Fig. 3.

For these geometric parameters, Table 2 gives the first eight natural frequencies for the perfect cylindrical panel without an elastic base and for the two cases of the elastic base shown in Fig. 3 [31]. The lowest natural frequencies always occur in the vibration mode (m, n) = (1, 1). As observed by Morais and Silva [31], Elastic Base 2 creates an internal resonance of type 1:2 between the vibration modes

Fig. 3 Positions on the cylindrical panel of the discontinuous elastic bases investigated here

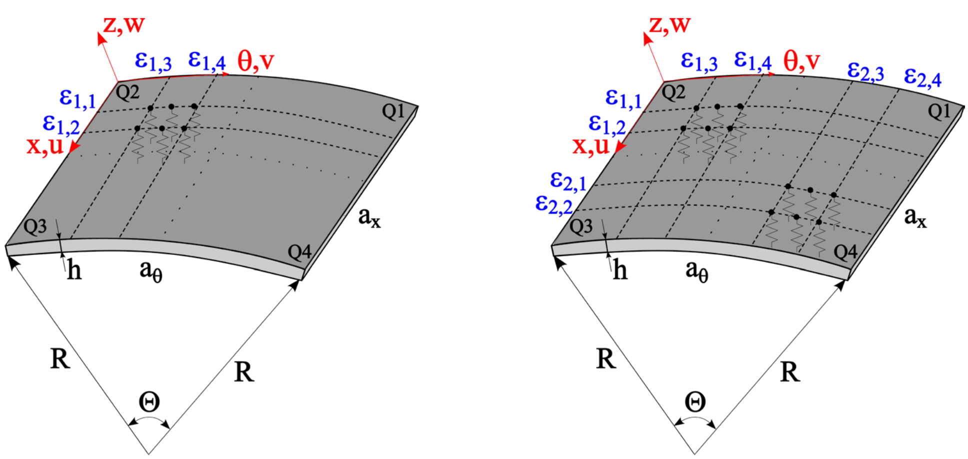

(a) Elastic Base 1, centered in quadrant Q2

(b) Elastic Base 2, centered in opposite quadrants Q2 and Q4

Table 1 Values for $\varepsilon_{i,1}$, $\varepsilon_{i,2}$, $\varepsilon_{i,3}$ and $\varepsilon_{i,4}$ (i=1, 2) for each case of the elastic base

Case	Contact area (%)	Longitudinal direction	Circumferential direction
Elastic base 1	7.5	$\varepsilon_{1,1}$=0.1130; $\varepsilon_{1,2}$=0.3870	$\varepsilon_{1,3}$=0.01356; $\varepsilon_{1,4}$=0.0464
	10.0	$\varepsilon_{1,1}$=0.0920; $\varepsilon_{1,2}$=0.4080	$\varepsilon_{1,3}$=0.0110; $\varepsilon_{1,4}$=0.0490
	12.5	$\varepsilon_{1,1}$=0.0732; $\varepsilon_{1,2}$=0.4268	$\varepsilon_{1,3}$=0.0068; $\varepsilon_{1,4}$=0.0512
Elastic base 2	7.5	$\varepsilon_{1,1}$=0.1130; $\varepsilon_{1,2}$=0.3870	$\varepsilon_{1,3}$=0.01356; $\varepsilon_{1,4}$=0.0464
		$\varepsilon_{2,1}$=0.6130; $\varepsilon_{2,2}$=0.8870	$\varepsilon_{2,3}$=0.07356; $\varepsilon_{2,4}$=0.1064
	10.0	$\varepsilon_{1,1}$=0.0920; $\varepsilon_{1,2}$=0.4080	$\varepsilon_{1,3}$=0.0110; $\varepsilon_{1,4}$=0.0490
		$\varepsilon_{2,1}$=0.5920; $\varepsilon_{2,2}$=0.9080	$\varepsilon_{2,3}$=0.0710; $\varepsilon_{2,4}$=0.1089
	12.5	$\varepsilon_{1,1}$=0.0732; $\varepsilon_{1,2}$=0.4268	$\varepsilon_{1,3}$=0.0068; $\varepsilon_{1,4}$=0.0512
		$\varepsilon_{2,1}$=0.5732; $\varepsilon_{2,2}$=0.9268	$\varepsilon_{2,3}$=0.0688; $\varepsilon_{2,4}$=0.1112

(m, n)=(1, 1) and (m, n)=(2, 1), whereas for Elastic Base 1, the internal resonance between these modes is almost 1:2. In addition, the elastic bases centered in the quadrant may be asymmetrically inserted, as in the case of Elastic Base 1, or antisymmetrically, as in the case of Elastic Base 2, giving rise to oscillations that excite the vibration modes with two half-waves in both the longitudinal and circumferential directions. Thus, to consider these important features and capture the correct nonlinear modal coupling between the vibration modes [31], we used the transversal modal solution in Eq. (10). This was obtained considering the modes $A_{1m,1n}(t)$ (i=j=1 in Eq. (8)) and $B_{2m,2n}(t)$ (α=β=0 in Eq. (8)) for each of the first four linear vibration modes of Table 2 (m=1, 2 and n=1, 2), giving a modal solution with eight degrees of freedom (8DOF), as follows:

$$w = \sum_{m=1,2}\sum_{j=1,2} A_{1m,1n}(t)\sin\left(\frac{m\pi x}{a_x}\right)\sin\left(\frac{n\pi\theta}{\Theta}\right) + \sum_{m=1,2}\sum_{n=1,2} B_{2m,2n}(t)\left\{\left[\frac{3}{4}-\cos\left(\frac{2m\pi x}{a_x}\right) + \frac{1}{4}\cos\left(\frac{4m\pi x}{a_x}\right)\right]\left[\frac{3}{4}-\cos\left(\frac{2n\pi\theta}{\Theta}\right)+\frac{1}{4}\cos\left(\frac{4n\pi\theta}{\Theta}\right)\right]\right\} \tag{10}$$

To discretize the nonlinear equilibrium equation for the cylindrical panel, the particular transverse displacement field in Eq. (10) was chosen and substituted into the compatibility and continuity equation in Eq. (2), which was then solved analytically. The value of f obtained in this way and the chosen value of w were then substituted into the nonlinear equilibrium equation in Eq. (1), and the Galerkin method was employed, with the harmonic functions of the modes of the transversal displacement field used as weight functions. In this way, a set of discretized second-order differential equations in terms of the modal amplitudes $A_{1m,1n}(t)$ and $B_{2m,2n}(t)$ was obtained, but this is omitted from this work due to its length and for ease of understanding.

The modal solution of Eq. (10) was then used to discretize the nonlinear equilibrium equation of the cylindrical panel in Eq. (1), and the resulting set of differential equations was solved using the MatCont package [49], a Matlab-based tool for numerical continuation and bifurcation analysis of ordinary differential equations that includes stability assessment via Floquet multipliers, to obtain the resonance curves. In some of the numerical analyses, phase portraits and Poincaré section mappings were also obtained through direct time integration of the discretized equilibrium equations using the classical fourth-order Runge–Kutta method. A constant time step equal to 1/100 of the panel's fundamental period was employed. Although adaptive time-step integration methods are often more appropriate for nonlinear and piecewise dynamic behavior, as displayed by the system investigated here, the classical Runge–Kutta method with a fixed time step provided sufficiently accurate results for the purposes of this study.

As shown in [31], Eq. (10) represents convergence of the nonlinear free vibration analysis. To verify this convergence for nonlinear forced analysis, Fig. 4 presents the

Table 2 First five natural frequencies (rad/s) and their ratio ω/ω_0 with respect to the lowest frequency value for a perfect cylindrical panel without elastic base and with the unilateral elastic bases investigated here [31] (Hypothesis 2)

Vibration mode		Without elastic base		Elastic base 1		Elastic base 2	
m	n	ω_0	ω/ω_0	ω_0	ω/ω_0	ω_0	ω/ω_0
1	1	437.91	1	464.66	1	496.19	1
1	2	782.30	1.79	815.83	1.76	858.67	1.73
2	1	918.23	2.10	950.47	2.05	987.70	2
2	2	1274.19	2.91	1314.31	2.83	1349.89	2.72
1	3	1546.01	3.53	1559.61	3.36	1573.68	3.17
3	1	1642.67	3.75	1655.52	3.56	1668.66	3.36
2	3	2017.26	4.61	2034.94	4.38	2052.80	4.14
3	2	2053.66	4.69	2069.64	4.45	2085.67	4.20

Poincaré section maps for perfect cylindrical panels with unilateral Elastic Bases 1 and 2, for the different modal solutions of Eq. (8). It also includes a comparison of the frequency–amplitude relationship (backbone curves) for a perfect cylindrical panel without an elastic base with results from Kobayashi [50]. It is worth noting that for a perfect cylindrical panel, w_0 is assumed to be zero, and the contact hypotheses presented in Fig. 2 remain the same. In this case, contact is represented by $w_r = w$ in Eq. (6). To obtain the nonlinear forced results, the following initial condition was considered: $A_{1m,1n}(t) = B_{2m,2n}(t) = 1e-4$ and $\dot{A}_{1m,1n}(t) = \dot{B}_{2m,2n}(t) = 0$ (m, n=1,2). From a qualitative point of view, it can be observed from this figure that these mappings present several paths with periodic responses of period 1 T interspersed by aperiodic responses, represented by the dispersed points in Fig. 4. All of the modal solutions investigated here adequately capture the bifurcation points that mark the transition from the periodic response to the aperiodic response. However, the modal solution with 6DOF is the only modal solution that shows greater dispersion of the point cloud at certain values of the excitation frequency. Hence, the modal solution composed of the modes with 8DOF, in Eq. (10), shows convergence for the transverse displacements for the two investigated elastic bases. Our convergence strategy is in line with the standard practices of nonlinear dynamics, as described in foundational works such as [51–53], which emphasize that the Poincaré map is the most effective tool for analyzing steady-state dynamics under periodic forcing and for identifying bifurcations. Also, to illustrate the convergence of dynamic stable response with the number of DOF, Fig. 4c–f depicted the time response of the modal amplitude of the fundamental vibration mode for the used models. According to these figures, the stable permanent response presents convergence increasing the number of DOF for both elastic bases and different frequency excitation that provokes periodicity 1T in the bifurcation diagrams of Fig. 4a, b.

The quality of the modal solution with 8DOF is also observed in the backbone curve for a perfect cylindrical panel without an elastic base, as shown in Fig. 4g. The backbone curve of Fig. 4g presents the same softening nonlinear behavior observed by Kobayashi [50]. In addition, the 8DOF modal solution is validated in Fig. 4h by comparison with the backbone curve obtained numerically from a finite element analysis. This curve was derived from a nonlinear time-domain simulation, in which small damping elements and initial conditions were incorporated corresponding to the first vibration mode shape with zero initial velocity. As shown in the figure, the nonlinear softening behavior predicted by the 8DOF modal solution is in good agreement with the finite element results, and gives better results than a 6DOF modal solution.

The following numerical results were obtained for values for the magnitude of the lateral load, damping factor and elastic base stiffness of P=2500 N/m^2, h_1=0.01 and K_w=92.30 MN/m^3, respectively, and a contact area of the elastic base equal to 7.5%, unless otherwise specified.

Figure 5 shows the resonance curves for the cylindrical panel with a bilateral elastic base in the panel quadrants shown in Fig. 3 and different initial geometrical imperfections. In this figure, the nonlinear forced behavior is almost linear for both cases of the elastic base. The initial geometric imperfections affect the amplitude of the main resonance peak, which decreases as the magnitude of the imperfection decreases. In the case of Elastic Base 1 (Fig. 5a), a secondary resonance peak becomes more pronounced with decreasing levels of imperfection, resulting in an unstable path delimited by the limit point cycle (LP).

The resonance curves for perfect cylindrical panels with unilateral contact (Elastic Bases 1 and 2) were obtained as shown in Fig. 6a, b, respectively. These figures reveal that the introduction of unilateral contact significantly alters the system's nonlinear dynamic behavior compared to the bilateral configuration presented in Fig. 5. More specifically, unilateral contact increases the number and complexity of the bifurcation points, including Neimark–Sacker (NS), LP, and period-doubling (PD) bifurcations, and creates a greater sensitivity to parameter variations. These bifurcations indicate transitions to more complex oscillatory regimes, and are associated with changes in stability along several branches of the resonance curves.

It can also be observed that the resonance curves for the unilateral cases are shifted to the left relative to the bilateral case. This frequency shift results from the intermittent nature of the contact between the structure and the elastic base, which modifies the effective stiffness during the vibration cycle. Since the contact is only partial (piecewise dynamic condition), the system effectively behaves as a softening oscillator in regions where detachment occurs.

To better understand the nature of these dynamic responses, Fig. 6c, d show the corresponding Poincaré sections for Fig. 6a, b, respectively. These mappings confirm that the unstable segments of the resonance curves are associated with quasiperiodic motion. In particular, the spread of the Poincaré points aligns with the unstable branches and the location of the NS bifurcations, thus reinforcing the link between these bifurcations and the onset of quasiperiodicity. An important implication of the appearance of quasiperiodic windows is the loss of continuity in some solution branches. These disconnected paths arise from the failure of numerical continuation techniques, such as those employed in MatCont, to converge in quasiperiodic regimes. This emphasizes the increased numerical complexity introduced by the unilateral constraint.

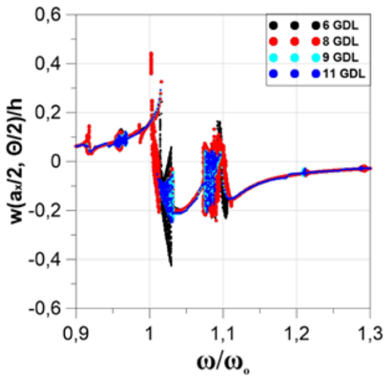

(a) Elastic Base 1

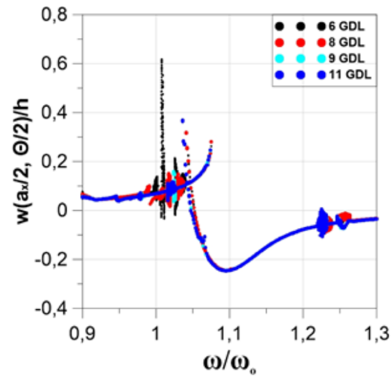

(b) Elastic Base 2

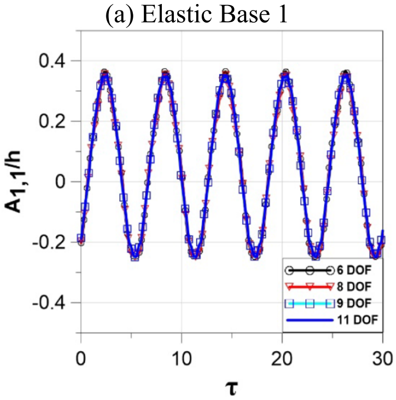

(c) Elastic Base 1 (ω/ω_0=0.95)

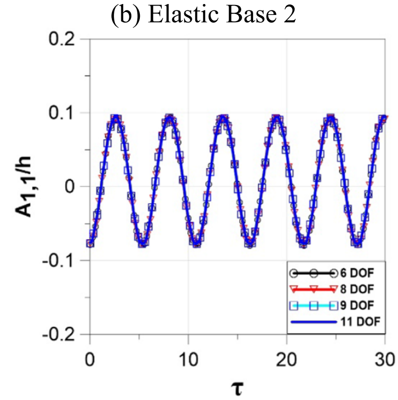

(d) Elastic Base 1 (ω/ω_0=1.15)

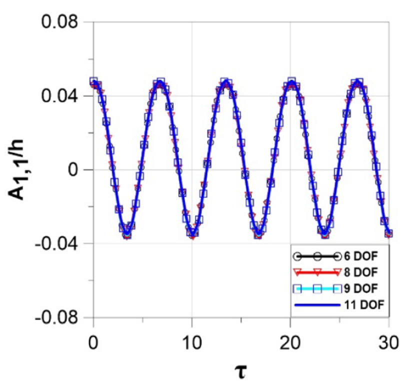

(e) Elastic Base 2 (ω/ω_0=0.95)

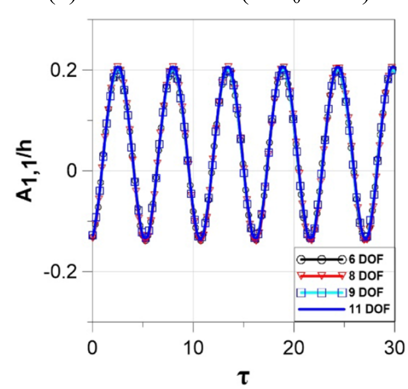

(f) Elastic Base 2 (ω/ω_0=1.15)

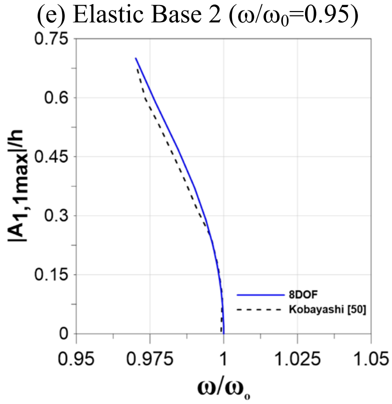

(g) Comparison of the backbone curve obtained here with results from Kobayashi [50]

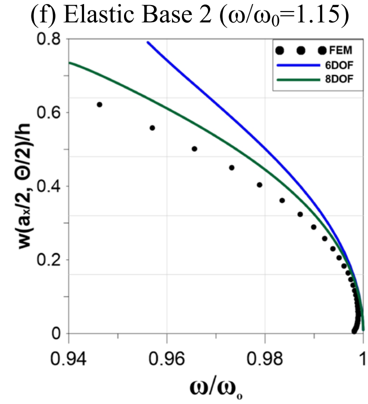

(h) Comparison of the backbone curve obtained here with results from finite element analysis

Fig. 4 Poincaré section mapping for perfect cylindrical panels with unilateral contact: **a** elastic base 1 and **b** elastic base 2, (P=2500 N/m^2, η_1=0.01, K_w=92.30 MN/m^3, contact area equal to 7.5%, direct time integration). Time response of permanent stable response considering **c**, **d** elastic base 1 and **e**, **f** elastic base 2 and **c**, **e** ω/ω_0=0.95, **d**, **f** ω/ω_0=1.15. Comparison of frequency-amplitude relations for a perfect panel without elastic base with results from **g** Kobayashi [50] and **h** finite element analysis. $A_{1,1}(t)$, $A_{1,2}(t)$, $A_{2,1}(t)$, $A_{2,2}(t)$, $B_{2,2}(t)$, $B_{8,2}(t)$; 8 DOF: 6DOF+$B_{2,8}(t)$, $B_{8,8}(t)$; 9DOF: 6DOF+$A_{1,3}(t)$, $A_{3,1}(t)$, $A_{3,3}(t)$; 11DOF: 8DOF+$A_{1,3}(t)$, $A_{3,1}(t)$, $A_{3,3}(t)$)

The richness of the dynamic behavior observed here is further illustrated in the phase portraits in Fig. 7, which show the transitions between different oscillatory regimes for unilateral contact (Elastic Base 1). Specifically, as the excitation frequency ratio ω/ω_0 increases, the system transitions from a quasiperiodic orbit, Fig. 7a, to a 1 T periodic orbit, Fig. 7b, and then to another quasiperiodic orbit, Fig. 7c. The quasiperiodic attractors in Fig. 7a–c represent unstable paths that lie between NS bifurcation points. This finding underscores the coexistence of multiple attractors and the strong influence of nonlinearity and piecewise dynamics on the overall system response.

The presence of the elastic base centered in the panel's quadrants Q2 excites the modal amplitudes $A_{1,2}(t)$, $A_{2,1}(t)$ and $A_{2,2}(t)$ in the region of the resonance region around the main resonance peak, as illustrated in Fig. 8a–c, demonstrating the influence of this asymmetrical elastic base on the nonlinear oscillations. Figure 8b shows that the vibration amplitude for mode $A_{2,1}(t)$ is greater than for modes $A_{1,2}(t)$ (Fig. 8a) and $A_{2,2}(t)$ (Fig. 8c). In contrast, for the antisymmetric elastic base positioned in quadrants Q2 and Q4, only the modal amplitude $A_{2,2}(t)$ is excited in the resonance region of the driven mode, as illustrated in Fig. 8d, demonstrating that this elastic base vibrates in only the antisymmetric mode with two wavenumbers in both the longitudinal and circumferential directions. The vibration of these modes plays an important role in the behavior of the nonlinear resonance curves, influencing the other resonance peaks and the several bifurcation points previously observed in the resonance curves of the driven mode $A_{1,1}(t)$ (Fig. 8a, b).

An initial geometric imperfection is introduced in the numerical analysis. As described in the previous section and shown in Fig. 2, the imperfection is considered in two scenarios, the difference between them being the reference used to calculate the work done by the reaction of the elastic base. Initially, the initial geometrical imperfection represented as Hypothesis 2, Fig. 2b, is considered to obtain the resonance curves of the cylindrical panel. In this case, there is no gap between the imperfect panel and the elastic base, ensuring that the panel is only detached from the elastic base during the positive phase of the vibrating cycle of the transversal displacements.

Figure 9 presents the resonance curves for imperfect cylindrical panels with both Elastic Bases 1 and 2, with geometric imperfections of magnitudes ±0.05 and ±0.10. To assess the influence of these geometric imperfections, the results for imperfect panels in Fig. 9a–d are compared with the perfect configuration for Elastic Base 1 (Fig. 6a). It is evident that the presence of imperfections significantly alters the dynamic response of the structure, introducing notable changes in the number and stability of the resonance branches.

For positive imperfections, an increase in the number of stable and unstable paths is observed, with the emergence of an NS bifurcation on the right side of the main resonance peak. This bifurcation indicates the onset of quasiperiodic behavior, which is not observed for the perfect panel. Conversely, negative imperfections lead to the formation of a secondary resonance peak around ω/ω_0=1.1, which is associated with a stable periodic response. This behavior replaces the quasiperiodic window observed at the same frequency for the perfect panel. These results demonstrate that imperfections do not merely perturb the resonance structure but can fundamentally alter the underlying bifurcation mechanisms and the nature of the system's attractors.

For Elastic Base 2 in Fig. 9e–h, the inclusion of imperfections induces comparatively minor changes in the resonance curves. The locations of the bifurcation points and the overall pattern of stable/unstable paths remain similar to those observed in the perfect configuration in Fig. 6b. This indicates that the influence of geometric imperfections is also strongly dependent on the characteristics of the elastic base and its interaction with the structure's unilateral constraints.

A key observation is related to the shift in the resonance peaks, which depends on the sign and magnitude of the imperfection. Due to the sensitivity of the natural frequencies to both the geometric imperfection and the unilateral elastic base [31], there is a rightward shift of the main resonance peak for panels with negative imperfections, Fig. 9a,b,e,f, relative to the perfect panel, whereas for positive imperfections, Fig. 9c,d,g,h, there is a leftward shift. This shift reflects the change in the effective stiffness induced by the imperfection and its interplay with the piecewise nature of the contact condition.

Overall, the inclusion of geometric imperfections in the analysis proves to be essential for capturing the full range of possible dynamic behaviors in cylindrical panels with unilateral elastic foundations. The results underscore the need for realistic modeling of imperfections in nonlinear structural dynamics, especially when bifurcations and stability transitions are of interest.

Figure 10 shows the phase portraits and Poincaré sections for the imperfect cylindrical panels investigated in Fig. 9 for chosen values of the excitation frequency that coincide with

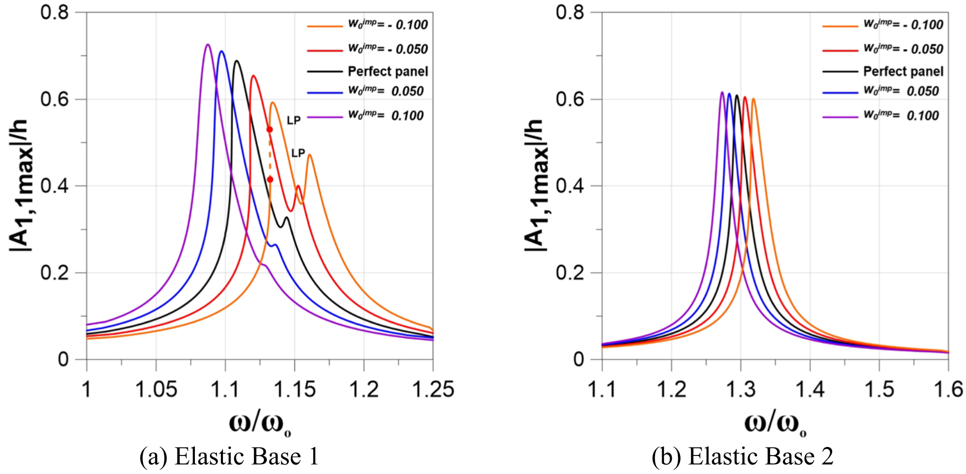

Fig. 5 Resonance curves for the cylindrical panel with bilateral contact: **a** Elastic base 1 and **b** Elastic base 2. (P=2500 N/m^2, η_1=0.01, K_w=92.30 MN/m^3, contact area equal to 7.5%, MatCont package)

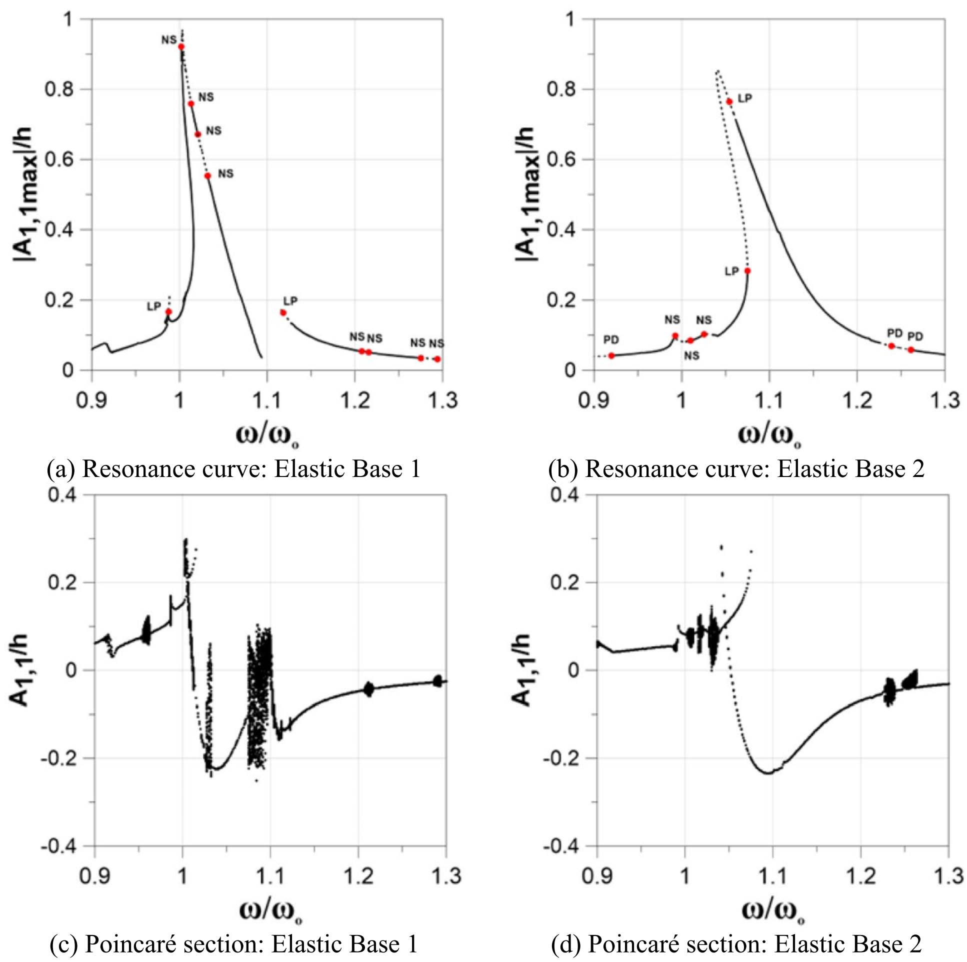

Fig. 6 **a**, **b** Resonance curves and **c**, **d** Poincaré section mapping for perfect cylindrical panels with unilateral contact **a**, **c** elastic base 1 and **b**, **d** elastic base 2. (P=2500 N/m^2, η_1=0.01, K_w=92.30 MN/m^3, contact area equal to 7.5%, **a**, **b** MatCont package and **c**, **d** direct time integration)

the nonresonant paths. This figure illustrates the changes in the orbits and the stability of the resonance curves in Fig. 9 as the magnitude of the imperfection is increased from −0.1 to 0.1. For the imperfect panel with Elastic Base 1 and the same excitation frequency ω/ω_0=1.03, as shown in Fig. 10a–d, an imperfection magnitude of −0.1 (Fig. 10a) leads to a stable periodic orbit with period 1 T. When the magnitude of the imperfection is increased to −0.05 (Fig. 10b) and 0.05 (Fig. 10c), the nonresonant orbits are unstable quasiperiodic orbits that can coexist with periodic stable orbits (Fig. 10b). When the magnitude of the imperfection is increased further to 0.1, the imperfect cylindrical panel again displays a periodically stable orbit (Fig. 10d). In contrast, for the imperfect panel with Elastic Base 2 and an excitation frequency of ω/

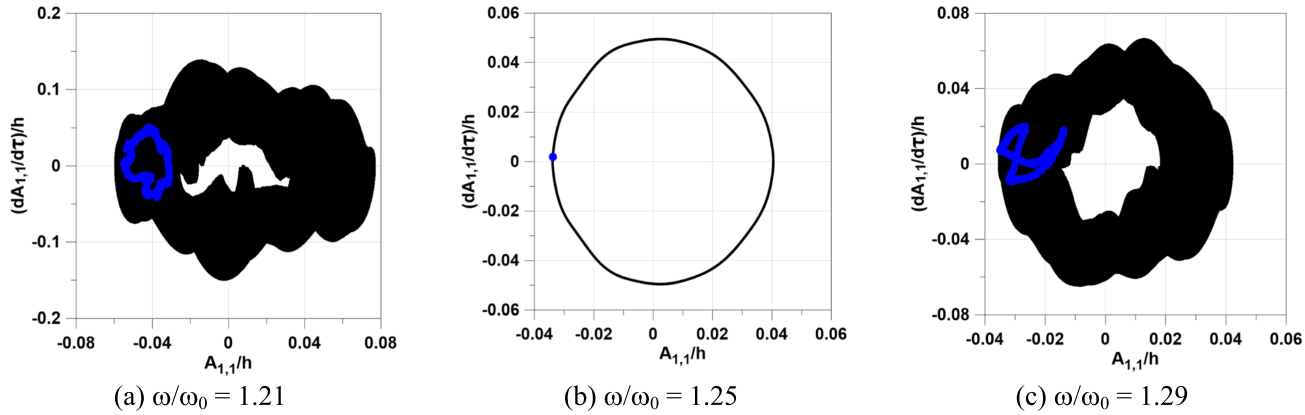

Fig. 7 Phase portraits and Poincaré sections for perfect cylindrical panels with unilateral contact (elastic base 1). (P=2500 N/m^2, η_1=0.01, K_w=92.30 MN/m^3, contact area equal to 7.5%, black lines—time response, blue dots—Poincaré section, direct time integration)

Fig. 8 Resonance curves for perfect cylindrical panels with unilateral contact: **a**–**c** elastic base 1 and **d** elastic base 2, for modal amplitudes **a**$A_{1,2}(t)$, **b**$A_{2,1}(t)$ and **c**, **d**$A_{2,2}(t)$. (P=2500 N/m^2, η_1=0.01, K_w=92.30 MN/m^3, contact area equal to 7.5%, MatCont package)

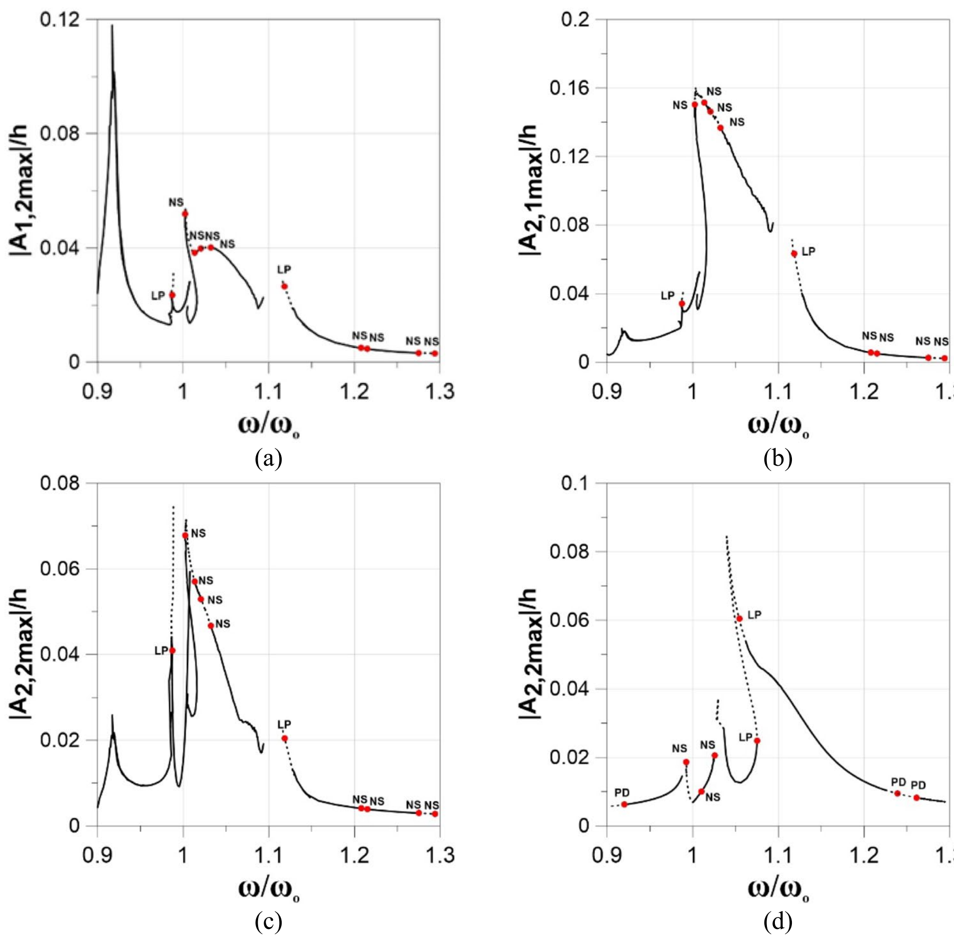

ω_0=1.10, as shown in Fig. 10e–h, the phase portraits display well-behaved periodic stable orbits with a period of 1 T as the magnitude of the imperfection increases. The orbits identified in Fig. 10 are in agreement with the resonance curves in Fig. 9.

Figure 11 illustrates the results for Hypothesis 1, defined in Fig. 2a, in terms of the resonance curves and Poincaré section mappings for various magnitudes of the imperfection and both Elastic Bases 1 and 2. These results were obtained through direct time integration, in which unstable branches are not explicitly identified. This limitation is due to the pronounced sensitivity of the system's dynamic response under this contact scenario, resulting in multiple regions dominated by quasiperiodic oscillations, regardless of the magnitude of the imperfection or the specific configuration of the elastic base. As shown in Fig. 11, the dynamic

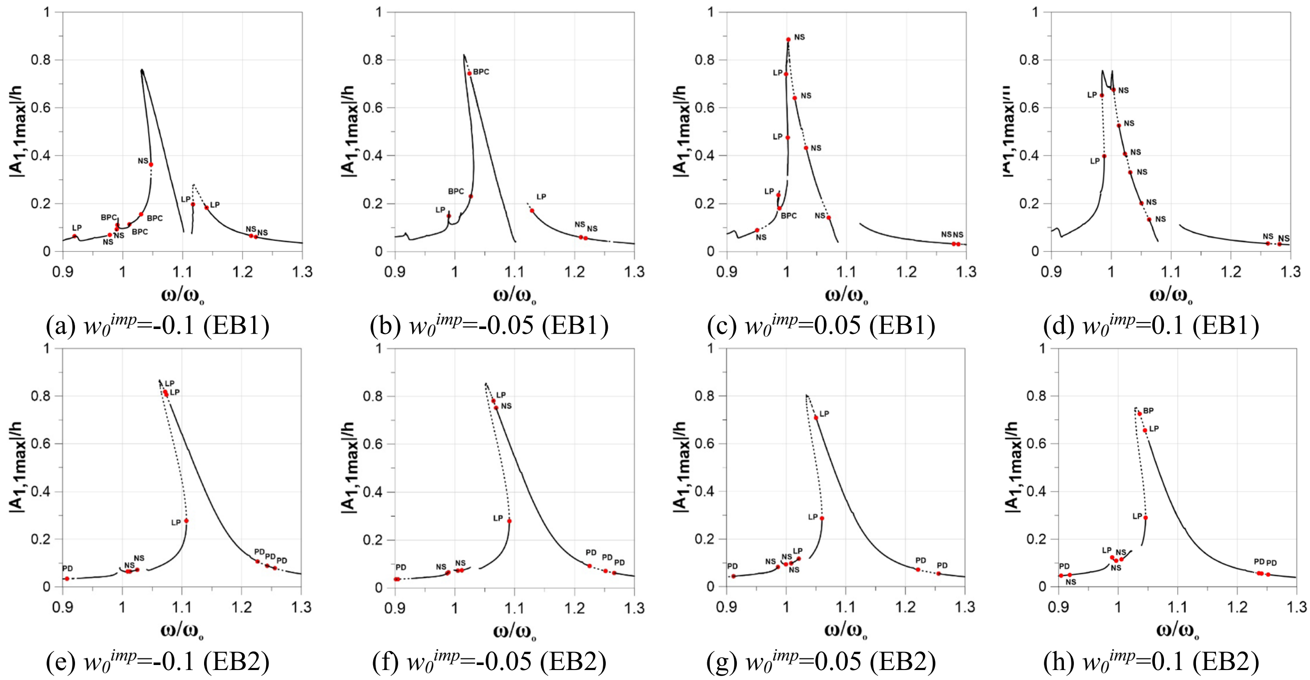

(a) w_0^{imp}=-0.1 (EB1) (b) w_0^{imp}=-0.05 (EB1) (c) w_0^{imp}=0.05 (EB1) (d) w_0^{imp}=0.1 (EB1)

(e) w_0^{imp}=-0.1 (EB2) (f) w_0^{imp}=-0.05 (EB2) (g) w_0^{imp}=0.05 (EB2) (h) w_0^{imp}=0.1 (EB2)

Fig. 9 Resonance curves for imperfect cylindrical panels with unilateral contact: **a**–**d** elastic base 1 (EB1) and **e**–**h** elastic base 2 (EB2), with varying magnitudes of the imperfection. (P=2500 N/m^2, η_1=0.01, K_w=92.30 MN/m^3, contact area equal to 7.5%, Hypothesis 2, MatCont package)

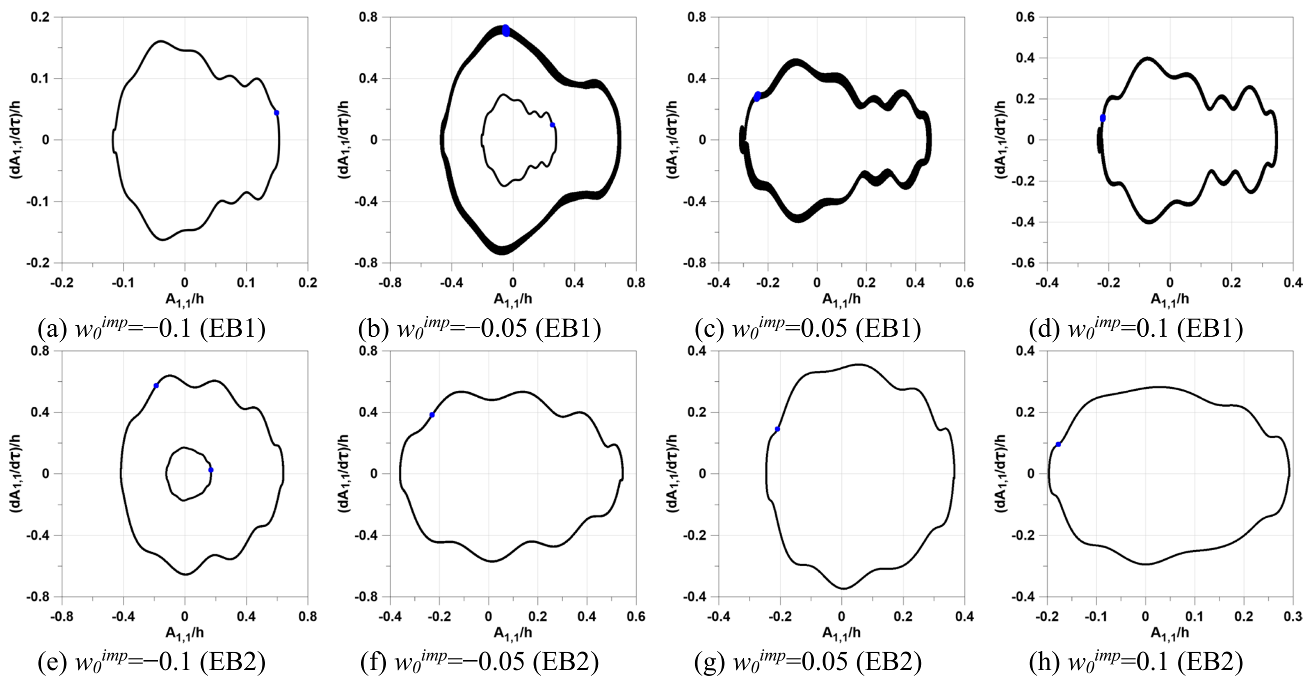

(a) w_0^{imp}=−0.1 (EB1) (b) w_0^{imp}=−0.05 (EB1) (c) w_0^{imp}=0.05 (EB1) (d) w_0^{imp}=0.1 (EB1)

(e) w_0^{imp}=−0.1 (EB2) (f) w_0^{imp}=−0.05 (EB2) (g) w_0^{imp}=0.05 (EB2) (h) w_0^{imp}=0.1 (EB2)

Fig. 10 Phase portraits and Poincaré sections for imperfect cylindrical panels with unilateral contact: **a**–**d** elastic base 1 (EB1) and **e**–**h** elastic base 2 (EB2), for **a**–**d** ω/ω_0 = 1.03 and **e**–**h** ω/ω_0 = 1.10. (P = 2500 N/m^2, η1 = 0.01, Kw = 92.30 MN/m^3, contact area equal to 7.5%, Hypothesis 2, black lines—time response, blue dots—Poincaré section, directtime integration)

behavior becomes highly fragmented, with resonant and non-resonant branches interspersed with stable periodic solutions and complex quasiperiodic responses. This pattern underscores the increased nonlinearity introduced by Hypothesis 1, which significantly modifies the nature of the contact between the panel and the elastic base.

One of the most critical effects of this hypothesis is the introduction of a gap between the panel and the elastic base,

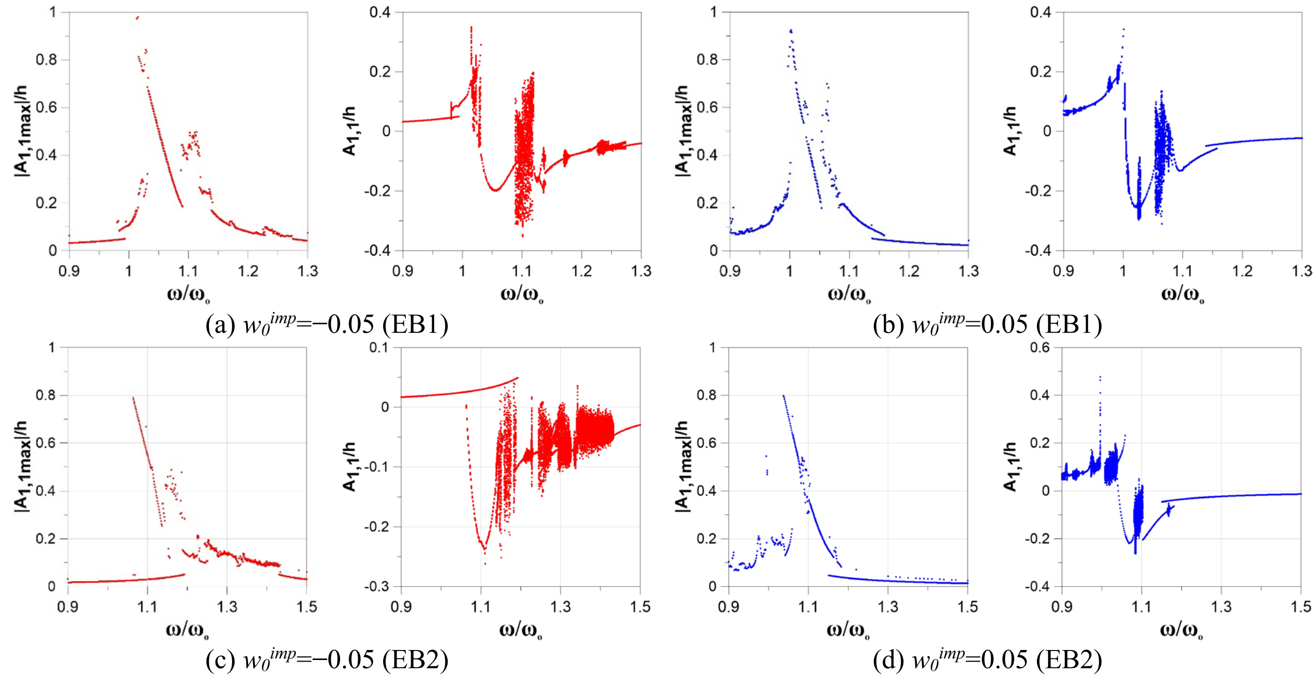

Fig. 11 Resonance curves and Poincaré section mapping for imperfect cylindrical panels with unilateral contact: **a**–**b** elastic base 1 (EB1) and **c**–**d** elastic base 2 (EB2) under contact conditions of Hypothesis 1 shown in Fig. 2a. (P=2500 N/m^2, η_1=0.01, K_w=92.30 MN/m^3, contact area equal to 7.5%, direct time integration)

particularly in the presence of positive imperfections. In such cases, the transverse displacement may reach negative values without initiating contact with the elastic base. This loss of contact delays the engagement of the elastic restoring force, altering both the stiffness profile and the energy transfer mechanisms within the system. In contrast, for negative imperfections, where the reference configuration is the perfect panel, the deformed geometry ensures that the panel maintains contact with the elastic base during the entire negative phase of the oscillation. As a result, the unilateral base is activated more frequently, leading to a stiffer dynamic response compared to the case of positive imperfection. This contrast directly influences the resonance characteristics and promotes different bifurcation behaviors and stability transitions.

The new contact conditions introduced by Hypothesis 1 therefore play a decisive role in shaping the nonlinear oscillatory behavior of the imperfect panel. When compared with the results under the original contact formulation, as shown in Fig. 10b,c,f,g, it becomes evident that the physical assumptions regarding activation of contact must be carefully considered. Even small changes in these assumptions can lead to substantial modifications to the system's resonance structure, stability properties, and the occurrence of complex dynamical regimes such as quasiperiodicity. This analysis emphasizes the importance of accurately modeling the interaction between the panel and the elastic base, especially when dealing with geometrically imperfect structures. The choice of contact hypothesis is not merely a modeling detail, but a key factor in predicting the full range of nonlinear dynamic phenomena.

To illustrate the influence of Hypothesis 1 on the resonance curves in Figs. 11, 12 shows some phase portraits and Poincaré sections for the imperfect cylindrical panel under this hypothesis of contact. For the panel with Elastic Base 1, shown in Fig. 12a, b, this scenario gives rise to quasiperiodic orbits for a magnitude of imperfection $w_0^{imp} = \pm 0.05$, and in the case where $w_0^{imp} = -0.05$, there is a stable periodic orbit of 1 T. Compared with the orbits in Fig. 10b, c, those in Fig. 12a, b are similar and independent of the contact scenarios illustrated in Fig. 2. In contrast, the phase portraits in Fig. 12c, d are different from those in Fig. 10f, g, showing a new stable periodic orbit with a low vibration amplitude coexisting with a large stable periodic orbit (Fig. 12c) and a quasiperiodic orbit (Fig. 12d).

The magnitude of the contact area of the elastic base was also investigated. Figure 13 shows the Poincaré section mapping and resonance curves obtained from direct time integration for an imperfect cylindrical panel with w_0^{imp}=0.05, for both Elastic Bases 1 and 2 and varying contact area of the elastic base. With increasing contact area, the behavior of the Poincaré section mapping remains very similar, independent of the type of elastic base (Fig. 13a–c and e–g), with several windows of quasiperiodic responses that intercalate periodic stable 1 T responses for each case of the elastic base. The main influence of the contact area is

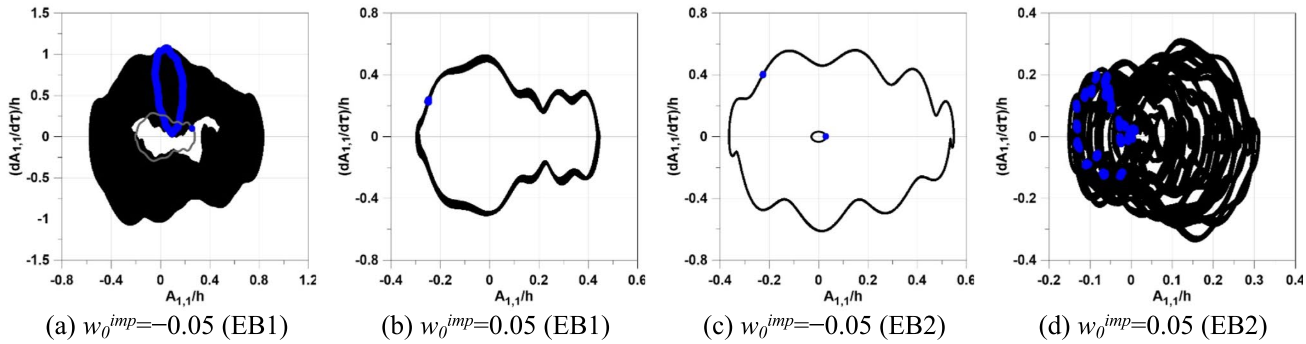

Fig. 12 Phase portraits and Poincaré sections for imperfect cylindrical panels with unilateral contact: **a**, **b** elastic base 1 (EB1) and **c**, **d** elastic base 2 (EB2), with **a**, **b** $\omega/\omega_0 = 1.03$ and **c**, **d** $\omega/\omega_0 = 1.10$. ($P = 2500$ N/m^2, $\eta_1 = 0.01$, $K_w = 92.30$ MN/m^3, contact area equal to 7.5%, Hypothesis 1, black lines—time response, blue dots—Poincaré section, direct time integration)

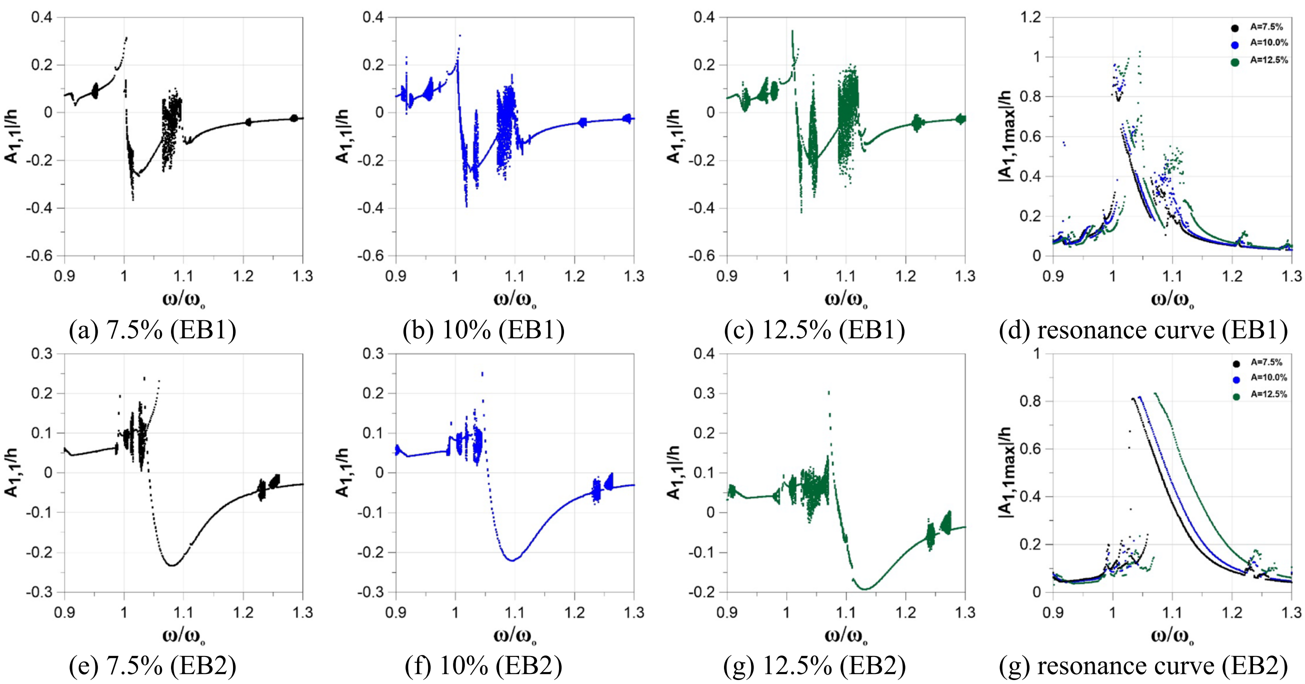

Fig. 13 **a**–**c**, **e**–**g** Poincaré section mapping and **d**, **h** resonance curves for imperfect cylindrical panels with unilateral contact: **a**–**d** elastic base 1 (EB1) and **e**–**h** elastic base 2 (EB2), with varying contact area for the elastic base. ($P = 2500$ N/m^2, $\eta_1 = 0.01$, $K_w = 92.30$ MN/m^3, $w_0^{imp} = 0.05$, Hypothesis 2, direct time-integration)

observed in the shifting of the resonance curves to the right (Fig. 13d, h) due to the changes in the natural frequency of the imperfect cylindrical panel with increasing contact area [31].

Finally, we investigated the influence of the contact area of the elastic base, under the conditions described in Hypothesis 2 for the contact interaction between the elastic base and the cylindrical panel, in order to better understand its role in the nonlinear dynamic behavior of the imperfect cylindrical panel. Figure 13 presents the resonance curves and corresponding Poincaré section mappings obtained via direct time integration for a panel with an imperfection magnitude of $w_0^{imp} = 0.05$, for both Elastic Bases 1 and 2, and a varying value of the contact area. The Poincaré sections in Fig. 13a–c and e–g reveal that despite variations in the contact area, the general structure of the dynamic response remains qualitatively similar for both types of elastic bases. In all cases, the response is characterized by alternating windows of quasiperiodic motion and stable periodic (1 T) solutions. This suggests that the system retains a complex nonlinear signature that is dominated by mode interactions and bifurcation phenomena intrinsic to the interaction between the panel and elastic base.

However, a significant and physically meaningful effect of increasing the contact area is observed in the resonance curves shown in Fig. 13d and h. As the contact area increases, the main resonance peak shifts to the right, indicating a rise in the effective stiffness of the system, and consequently an increase in the natural frequency of the imperfect panel. This behavior is consistent with previous findings [31] in which extension of the contact region leads to a greater portion of the panel being constrained during vibration, thus effectively reinforcing the system and modifying its inertial–stiffness balance. These results highlight the critical role of the contact area parameter in the design of nonlinear structural systems with unilateral foundations. Although the contact area does not significantly alter the qualitative nature of the dynamic attractors, as shown by the Poincaré maps, it plays a fundamental role in shaping the quantitative characteristics of the system, particularly in terms of tuning the resonance frequencies and influencing the overall stiffness of the imperfect panel–elastic base assembly. It is worth noting that both the stiffness of the elastic foundation and the size of the contact area can affect the convergence of the modal solution used in Eq. (10), potentially requiring the inclusion of additional terms. In this manuscript, convergence of the modal solution with 8DOF is ensured for the stiffness of the elastic foundation considered here and for contact areas smaller than 12.5%, as shown in Fig. 4.

4 Concluding remarks

In this work, the influence of a discontinuous unilateral elastic force on the nonlinear resonance behavior of simply supported imperfect cylindrical panels was investigated. Our semi-analytical model was developed from a set of nonlinear partial differential equilibrium equations, in which Donnell's shallow shell theory for the transverse displacement was combined with Airy's stress function for in-plane stress fields. These equations were discretized via the Galerkin method, with a consistent modal expansion for the transverse displacement field, previously obtained through a perturbation technique [31]. The effects of the discontinuous unilateral elastic foundation were incorporated directly into the nonlinear equilibrium equation using Heaviside and signum functions, thereby enabling the modeling of localized and non-smooth contact behavior. Numerical strategies were applied to compute nonlinear resonance curves, phase portraits, and Poincaré sections, considering variations in the initial geometric imperfections and the parameters defining the elastic base (location, contact area, and type of contact). Numerical results showed that the inclusion of unilateral contact significantly alters the stability of the resonance curves, with multiple NS, period-doubling, and limit-cycle bifurcations being introduced due to the intermittent engagement of the elastic base during the vibration cycle. The system exhibited strong sensitivity to excitation frequency under the assumption of unilateral contact. Moreover, the initial geometric imperfections had a substantial impact on the resonance behavior, in terms of modifying stability boundaries and increasing the extent of unstable response paths. The presence of an initial gap between the shell and the foundation further intensified the system's sensitivity, introducing additional bifurcation points and amplifying the complexity of the stable/unstable dynamics. Finally, the position of the resonance peaks was found to depend strongly on the magnitude of the imperfection, the characteristics of the contact (unilateral or bilateral), and the effective contact area of the elastic base.

Acknowledgements This study was financed in part by the Coordenação de Aperfeiçoamento de Pessoal de Nível Superior – Brazil (CAPES) – Finance Code 001.

Author contribution Jordana L. Morais: Methodology, software, validation, formal analysis, visualization, writing- original draft. Frederico M. A. Silva: Conceptualization, software, data curation, resources, funding acquisition, writing- reviewing and editing.

Funding The Article Processing Charge (APC) for the publication of this research was funded by the Coordenação de Aperfeiçoamento de Pessoal de Nível Superior - Brasil (CAPES) (ROR identifier: 00x0ma614).

Data availability This manuscript has no associated data.

Declarations

Conflict Of interest The authors declare that there is no conflict of interest regarding the publication of this paper.

5. References

1. Wang YH, Tham LG, Cheung YK (2005) Beams and plates on elastic foundations: a review. Prog Struct Eng Mater. https://doi.org/10.1002/pse.202
2. Younesian D, Hosseinkhani A, Askari H, Esmailzadeh E (2019) Elastic and viscoelastic foundations: a review on linear and nonlinear vibration modeling and applications. Nonlinear Dyn 97:853–895. https://doi.org/10.1007/s11071-019-04977-9
3. Zhao X, Zhu WD, Li YH, Li M, Li XY (2022) Review, classification, and extension of classical soil-structure interaction models based on different superstructures and soils. Thin-Walled Struct 173:108936. https://doi.org/10.1016/j.tws.2022.108936

4. Lamprea-Pineda AC, Connolly DP, Hussein MFM (2022) Beams on elastic foundations—a review of railway applications and solutions. Transp Geotech 33:100696. https://doi.org/10.1016/j.trgeo.2021.100696
5. Malekjafarian A, Jalilvand S, Doherty P, Igoe D (2021) Foundation damping for monopile supported offshore wind turbines: a review. Mar Struct 77:102937. https://doi.org/10.1016/j.marstruc.2021.102937
6. Liew KM, Lim CW, Kitipornchai S (1997) Vibration of shallow shells: a review with bibliography. Appl Mech Rev 50:431–444. https://doi.org/10.1115/1.3101731
7. Sandeep SH, Srinivasa CV (2020) Hybrid sandwich panels: a review. Int J Appl Mech Eng 25:64–85. https://doi.org/10.2478/ijame-2020-0035
8. Moussaoui F, Benamar R (2002) Non-linear vibrations of shell-type structures: a review with bibliography. J Sound Vib. https://doi.org/10.1006/jsvi.2001.4146
9. Alijani F, Amabili M (2014) Non-linear vibrations of shells: a literature review from 2003 to 2013. Int J Non-Linear Mech 58:233–257. https://doi.org/10.1016/j.ijnonlinmec.2013.09.012
10. Amabili M, Païdoussis MP (2003) Review of studies on geometrically nonlinear vibrations and dynamics of circular cylindrical shells and panels, with and without fluid-structure interaction. Appl Mech Rev 56:349–356. https://doi.org/10.1115/1.1565084
11. Amabili M, Dalpiaz G (1997) Free vibrations of cylindrical shells with non-axisymmetric mass distribution on elastic bed. Meccanica 32:71–84. https://doi.org/10.1023/A:1004219803239
12. Paliwal DN, Pandey RK, Nath T (1996) Free vibrations of circular cylindrical shell on Winkler and Pasternak foundations. Int J Press Vessels Piping. https://doi.org/10.1016/0308-0161(95)00010-0
13. Gunawan Tj H, Mikami T, Kanie S, Sato M (2005) Free vibrations of fluid-filled cylindrical shells on elastic foundations. Thin-Walled Struct 43:1746–1762. https://doi.org/10.1016/j.tws.2005.07.005
14. Gunawan Tj H, Mikami T, Kanie S, Sato M (2006) Free vibration characteristics of cylindrical shells partially buried in elastic foundations. J Sound Vib 290:785–793. https://doi.org/10.1016/j.jsv.2005.04.014
15. Bakhtiari-Nejad F, Mousavi Bideleh SM (2012) Nonlinear free vibration analysis of prestressed circular cylindrical shells on the Winkler/Pasternak foundation. Thin-Walled Struct 53:26–39. https://doi.org/10.1016/j.tws.2011.12.015
16. Duc ND, Hadavinia H, Van Thu P, Quan TQ (2015) Vibration and nonlinear dynamic response of imperfect three-phase polymer nanocomposite panel resting on elastic foundations under hydrodynamic loads. Compos Struct 131:229–237. https://doi.org/10.1016/j.compstruct.2015.05.009
17. Duc ND, Kim S-E, Manh DT, Nguyen PD (2020) Effect of eccentrically oblique stiffeners and temperature on the nonlinear static and dynamic response of S-FGM cylindrical panels. Thin-Walled Struct 146:106438. https://doi.org/10.1016/j.tws.2019.106438
18. Silva FMA, Rodrigues PC, Gonçalves PB (2020) Nonlinear oscillation of a FG cylindrical shell on a discontinuous elastic foundation. In: B.B. Lacarbonara W., Ma J., Tenreiro Machado J., Stepan G. (ed) New trends in nonlinear dynamics. Springer, Cham. https://doi.org/10.1007/978-3-030-34724-6_9
19. Pereira JKA, Soares RM, Silva FMA, Gonçalves PB (2023) Nonlinear oscillations of a cylindrical shell with a circumferentially discontinuous elastic base. Int J Non-Linear Mech 155:104475. https://doi.org/10.1016/j.ijnonlinmec.2023.104475
20. Shaw SW, Holmes PJ (1983) A periodically forced piecewise linear oscillator. J Sound Vib 90:129–155. https://doi.org/10.1016/0022-460X(83)90407-8
21. Chicurel-Uziel E (2001) Exact, single equation, closed-form solution of vibrating systems with piecewise linear springs. J Sound Vib 245:285–301. https://doi.org/10.1006/jsvi.2001.3568
22. Lancioni G, Lenci S (2007) Forced nonlinear oscillations of a semi-infinite beam resting on a unilateral elastic soil: analytical and numerical solutions. J Comput Nonlinear Dyn 2:155–166. https://doi.org/10.1115/1.2447406
23. Lenci S, Clementi F (2020) Flexural wave propagation in infinite beams on a unilateral elastic foundation. Nonlinear Dyn 99:721–735. https://doi.org/10.1007/s11071-019-04944-4
24. Coskun I, Engin H (1999) Non-linear vibrations of a beam on an elastic foundation. J Sound Vib 223:335–354. https://doi.org/10.1006/jsvi.1998.1973
25. Bhattiprolu U, Bajaj AK, Davies P (2016) Periodic response predictions of beams on nonlinear and viscoelastic unilateral foundations using incremental harmonic balance method. Int J Solids Struct 99:28–39. https://doi.org/10.1016/j.ijsolstr.2016.08.009
26. Panahandeh-Shahraki D, Mirdamadi HR (2014) Shell–tensionless foundation interaction and nonlinear thermoelastic stability analysis of laminated composite cylindrical panels. Acta Mech 225:131–149. https://doi.org/10.1007/s00707-013-0943-x
27. Silveira RAM, Pereira WLA, Gonçalves PB (2008) Nonlinear analysis of structural elements under unilateral contact constraints by a Ritz type approach. Int J Solids Struct 45:2629–2650. https://doi.org/10.1016/j.ijsolstr.2007.12.012
28. Casini P, Vestroni F (2011) Characterization of bifurcating nonlinear normal modes in piecewise linear mechanical systems. Int J Non-Linear Mech 46:142–150. https://doi.org/10.1016/j.ijnonlinmec.2010.08.002
29. Vestroni F, Luongo A, Paolone A (2008) A perturbation method for evaluating nonlinear normal modes of a piecewise linear two-degrees-of-freedom system. Nonlinear Dyn 54:379–393. https://doi.org/10.1007/s11071-008-9337-3
30. Giannini O, Casini P, Vestroni F (2011) Experimental evidence of bifurcating nonlinear normal modes in piecewise linear systems. Nonlinear Dyn 63:655–666. https://doi.org/10.1007/s11071-010-9827-y
31. Morais JL, Silva FMA (2024) Nonlinear free vibration analysis of imperfect cylindrical panels with discontinuous unilateral elastic base. Int J Non-Linear Mech 167:104884. https://doi.org/10.1016/j.ijnonlinmec.2024.104884
32. Morais JL, Silva FMA (2019) Influence of modal coupling and geometrical imperfections on the nonlinear buckling of cylindrical panels under static axial load. Eng Struct 183:816–829. https://doi.org/10.1016/J.ENGSTRUCT.2018.12.032
33. Amabili M (2008) Nonlinear vibrations and stability of shells and plates. Cambridge University Press, Cambridge
34. Donnell LH, OHIO A (1934) A new theory for the buckling of thin cylinders under axial compression and bending, ASME - Aeronautical Engineering AER-56-12, pp 795–806
35. Pellicano F, Barbieri M (2014) Complex dynamics of circular cylindrical shells. Int J Non Linear Mech 65:196–212. https://doi.org/10.1016/j.ijnonlinmec.2014.05.006
36. Amabili M (2005) Nonlinear vibrations of circular cylindrical panels. J Sound Vib 281:509–535. https://doi.org/10.1016/J.JSV.2004.01.021
37. Gonçalves PB, del Prado ZG (2004) Effect of non-linear modal interaction on the dynamic instability of axially excited cylindrical shells. Comput Struct 82:2621–2634. https://doi.org/10.1016/j.compstruc.2004.04.020
38. Gonçalves PB, Del Prado ZJGN (2002) Nonlinear oscillations and stability of parametrically excited cylindrical shells. Meccanica. https://doi.org/10.1023/A:1020972109600
39. Gonçalves PB, Del Prado ZJGN (2005) Low-dimensional Galerkin models for nonlinear vibration and instability analysis of

cylindrical shells. Nonlinear Dyn. https://doi.org/10.1007/s11071-005-2802-3
40. Gonçalves PB, Silva FMA, Del Prado ZJGN (2008) Low-dimensional models for the nonlinear vibration analysis of cylindrical shells based on a perturbation procedure and proper orthogonal decomposition. J Sound Vib 315:641–663. https://doi.org/10.1016/J.JSV.2008.01.063
41. Gonçalves PB, Silva FMA, Del Prado ZJGN (2016) Reduced order models for the nonlinear dynamic analysis of shells. Procedia IUTAM 19:118–125. https://doi.org/10.1016/J.PIUTAM.2016.03.016
42. Rodrigues L, Silva FMA, Gonçalves PB, Del Prado ZJGN (2014) Effects of modal coupling on the dynamics of parametrically and directly excited cylindrical shells. Thin Walled Struct 81:210–224. https://doi.org/10.1016/J.TWS.2013.08.004
43. Rodrigues L, Silva FMA, Gonçalves PB (2022) Effect of geometric imperfections and circumferential symmetry on the internal resonances of cylindrical shells. Int J Non-Linear Mech 139:103875
44. Rodrigues L, Silva FMA, Gonçalves PB (2020) Influence of initial geometric imperfections on the 1:1:1:1 internal resonances and nonlinear vibrations of thin-walled cylindrical shells. Thin-Walled Struct. https://doi.org/10.1016/j.tws.2020.106730
45. Silva FMA, Vaz WA, Gonçalves PB (2020) Internal resonances in an imperfect circular cylindrical panel. In: Nonlinear dynamics of structures, systems and devices, Springer, Cham, pp 179–186. https://doi.org/10.1007/978-3-030-34713-0_18
46. Silva FMA, Sattler HAR, Gonçalves PB, del Prado ZJGN (2016) Influence of modal coupling on the nonlinear vibration of simply supported cylindrical panels. Appl Mech Mater 849:106–118. https://doi.org/10.4028/www.scientific.net/AMM.849.106
47. Jansen EL (2005) Dynamic stability problems of anisotropic cylindrical shells via a simplified analysis. Nonlinear Dyn 39:349–367. https://doi.org/10.1007/s11071-005-4343-1
48. Gonçalves PB, Del Prado ZJGN (2000) The role of modal coupling on the non-linear response of cylindrical shells subjected to dynamic axial loads. In: Nonlinear dynamics of shells and plates, american society of mechanical engineers, pp 105–116. https://doi.org/10.1115/IMECE2000-1010.
49. Govaerts W, Kuznetsov YA, Meijer HGE, Al-Hdaibat B, De Witte V, Dhooge A, Mestrom W, Neirynck N, Riet AM, Sautois B (2020) MATCONT: continuation toolbox for ODEs in Matlab, Retrieved December 4 (2019)
50. Kobayashi Y, Leissa AW (1995) Large amplitude free vibration of thick shallow shells supported by shear diaphragms. Int J Non-Linear Mech 30:57–66. https://doi.org/10.1016/0020-7462(94)00030-E
51. Nayfeh AH, Mook DT (1979) Nonlinear oscillations. Wiley, New York
52. Guckenheimer J, Holmes P (1983) Nonlinear oscillations, dynamical systems, and bifurcations of vector fields. Springer, New York
53. Kovacic I, Brennan MJ (2011) The duffing equation: nonlinear oscillators and their behaviour. Wiley, Chichester